

Synthesis and Photochemical Properties of Novel Ruthenium(II)-Nickel(II) and Ruthenium(II)-Copper(II) Dinuclear Complexes

Nobuko Onozawa-Komatsuzaki, Ryuzi Katoh, Yuichiro Himeda, Hideki Sugihara, Hironori Arakawa, and Kazuyuki Kasuga*

Photoreaction Control Research Center, National Institute of Advanced Industrial Science and Technology (AIST), Tsukuba Central 5, 1-1-1 Higashi, Tsukuba, Ibaraki 305-8565

(Received September 30, 2002)

Novel Ru(II)-Ni(II) and Ru(II)-Cu(II) dinuclear complexes have been synthesized and characterized. In these complexes, the ruthenium(II) polypyridyl group and the Ni(II)- or Cu(II)-Schiff base units are fused together by a bridging ligand, 5,6-di(salicylidenamino)-1,10-phenanthroline. X-ray crystallography on the Ru(II)-Ni(II) dinuclear complex shows that the Ni(II)-Schiff base unit is distorted against the plane of the phenanthroline ring due to the effect of a steric repulsion between the phenanthroline ring and the Ni(II)-Schiff base unit. The properties of the excited states of the dinuclear complexes are discussed by comparing them with that of the Ru(II)-Zn(II) analogue as a reference compound. These complexes show the emission from the excited state, which is assigned to $MLCT_0$ (the excited state due to the transition from Ru(II) to the bridging ligand). For the Ru(II)-Cu(II) complex, the lifetime of the emission is found to be 80 ns, which is identical to that of the Ru(II)-Zn(II) analogue, suggesting that no quenching process exists. On the contrary, for the Ru(II)-Ni(II) complex, the emission decays very rapid. The energy transfer to the Ni(II)-Schiff base unit deactivates the $MLCT_0$ excited state.

Much attention has been devoted to the synthesis of polynuclear complexes which conduct the effective intramolecular electron- or energy-transfer.[1] Especially, polynuclear complexes incorporating the ruthenium(II) polypyridyl group are very interesting,[2] since the ruthenium(II) polypyridyl group has several attractive properties as a photosensitizer and/or an electron mediator.[3] Hence, many kinds of such polynuclear systems have so far been studied in terms of their photo and/or redox properties.[4] Although most of these studies have been focused on the basic properties of the complexes, some of them have been utilized as functional materials,[5] such as photochemical molecular devices[6] and metallopolymer.[7] Moreover, there are few reports on photochemical reactions using such polynuclear complexes.[8]

In our recent paper, we reported on the Ru(II)-Co(III) and Ru(II)-Ni(II) dinuclear complexes in which two metal centers are covalently linked by a bisphenanthroline ligand.[9] In these complexes, we expected that the electron acceptor parts, Co(III) or Ni(II) center, act as a catalyst for CO_2 reduction. Actually, these complexes showed a catalytic ability for the photoreduction of CO_2, though their efficiencies were not high. In order to realize systems with high efficiency, one must fulfill several necessary criteria, such as high stabilization of the charge-separated intermediate, high reactivity of the catalytic part and so on.[10] From this point of view, we continued our research on the design and synthesis of novel photoactive polynuclear complexes.

A metal-Schiff base complex might be an interesting candidate as a component for constructing such photoactive polynuclear systems, since it is expected to act as an electron donor or acceptor in such systems.[11] Furthermore, some metal-Schiff base complexes have been used as catalysts.[12–15] For example, some manganese(III)-Schiff base complexes catalyze the asymmetric epoxidation[12] and oxidation of water.[13] Some cobalt(II)-Schiff base complexes can fix CO_2[14] and act as a catalyst for electrochemical CO_2 reduction.[15]

In this paper, we report on the synthesis and photochemical properties of novel Ru(II)-Ni(II) and Ru(II)-Cu(II) dinuclear complexes, in which the ruthenium(II) polypyridyl group and the Ni(II)- or Cu(II)-Schiff base units are fused together by a bridging ligand, 5,6-di(salicylidenamino)-1,10-phenanthroline.[16] In these dinuclear complexes, the intramolecular energy or electron-transfer through the metal-Schiff base unit can be expected to occur. In order to elucidate the precise photophysical behavior of the complexes, laser flash-photolysis techniques were used. A Ru(II)-Zn(II) analogue was prepared as a reference compound, and its photochemical properties were compared with those of the Ru(II)-Ni(II) and Ru(II)-Cu(II) dinuclear complexes. Based on the results of these studies, the possibility of the utilization for photoreactions was also considered.

Results and Discussion

Synthesis of the Dinuclear Complexes. The synthetic route of the complexes is summarized in Scheme 1. 5,6-Diamino-1,10-phenanthroline was used for bridging between two metals, and its ruthenium(II) complex **1** was prepared by a reported method.[17] The dinuclear complexes **2a–c** were synthesized in one pot by reacting two equivalents of salicylaldehyde with nickel(II), copper(II) or zinc(II) acetate and **1** in ethanol. This reaction needed a longer reaction time and a higher temperature than those necessary for preparing common

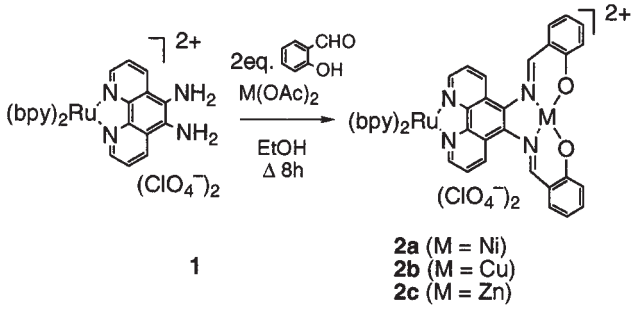

Scheme 1. Synthesis of the Ru(II)-Ni(II), Ru(II)-Cu(II) and Ru(II)-Zn(II) dinuclear complexes.

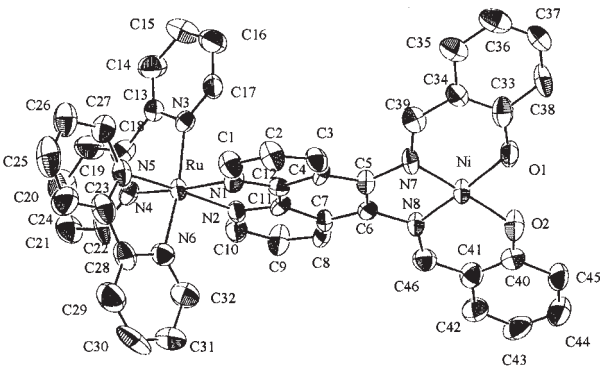

Fig. 1. ORTEP drawing of **2a** (hydrogen atoms and ClO_4 are not shown for clarity).

metal-Schiff base complexes. This may be attributed to the low nucleophilicity of the diamino groups caused by the electron-withdrawing effect of the cationic ruthenium(II) ion and the strain of the metal-Schiff base ligand formed. The obtained complexes **2a**,**b** were characterized by elemental analysis, NMR and ES-Mass spectroscopies. The ^{1}H NMR spectrum of **2a** in CD_3CN showed a singlet at 8.44 ppm, which was assigned to the two imide protons in the metal-Schiff base part, though a ^{1}H NMR measurement was impossible for **2b** due to the paramagnetic character of the Cu(II) ion. On the other hand, **2c** was obtained in low yield, and could not be purified thoroughly because of its instability.

Attempts to synthesize the same type complexes containing other metal-Schiff base units, such as Co(II), were unsuccessful. Furthermore, when the reaction of **1** with salicylaldehyde was carried out without metal acetates, a mononuclear ruthenium(II) complex containing the Schiff-base ligand could not be obtained. This clearly demonstrates that the template effect of metal ions is important for constructing the metal-Schiff base unit in these complexes.

Crystal Structure of 2a. Recrystallization of **2a** from C_2H_5OH–CH_3CN gave crystals suitable for X-ray crystallography. An ORTEP drawing of **2a** with an atomic numbering scheme is illustrated in Fig. 1. The crystal data and the experimental details are listed in Table 1. Selected bond lengths and angles are summarized in Table 2. In the dinuclear complex **2a**, the Ni(II)-Schiff base unit is distorted against the plane of the phenanthroline ring due to the effect of a steric repulsion between the phenanthroline ring and the Ni(II)-Schiff base unit. A dihedral angle of 23.5° is formed between the plane of the phenanthroline ring (C(4–7)–C(11,12)) and the plane of the Ni(II)-Schiff base unit (C(5)–C(6)–N(8)–Ni–N(7)). The ruthenium center has a slightly distorted octahedral configuration. The bond angle of N(1)–Ru–N(2) is 78.6(5)°, which is smaller than that of N(4)–Ru–N(5) (87.4(5)°) with the average Ru–N

Table 1. Crystal Data and Parameters of Data Collection for Complex **2a**

Formula	$C_{46}H_{32}N_8O_{10}Cl_2RuNi \cdot H_2O$
Molecular weight	1105.50
Crystal system	Triclinic
Space group	$P\bar{1}$
a/Å	9.525(2)
b/Å	12.208(3)
c/Å	20.436(5)
α/°	96.69(2)
β/°	90.55(2)
γ/°	99.94(2)
V/Å^3	2323.5(9)
Z	2
F(000)	1099
D_c/g cm^{-3}	1.55
Colour	Orange
μ/mm^{-1}	9.053
Crystal size/mm	0.45 × 0.10 × 0.20
T/K	298
Radiation (λ/Å)	Mo Kα (0.71073)
Refinement on F	
No. measured reflections	8679
No. independent reflections	8172
No. reflections in refinement	3788 ($\|F_o\| \geq 3\sigma\|F_o\|$)
No. variables	622
Final R	0.068
Final R_w	0.108
Maximum, minimum in electron density difference map/e Å^{-3}	1.24, −0.59

Table 2. Selected Bond Lengths (Å) and Angles (°) of **2a**

Ru–N(1)	2.07(1)	Ru–N(2)	2.04(1)
Ru–N(3)	2.07(1)	Ru–N(4)	2.04(1)
Ru–N(5)	2.07(1)	Ru–N(6)	2.05(1)
Ni–O(1)	1.84(1)	Ni–O(2)	1.84(1)
Ni–N(7)	1.87(1)	Ni–N(8)	1.84(1)
O(1)–C(33)	1.31(3)	O(2)–C(40)	1.32(2)
N(7)–C(5)	1.42(2)	N(7)–C(39)	1.32(2)
N(8)–C(6)	1.43(2)	N(8)–C(46)	1.31(2)
N(1)–Ru–N(2)	78.6(5)	N(1)–Ru–N(3)	93.9(5)
N(1)–Ru–N(4)	172.6(5)	N(1)–Ru–N(5)	97.6(5)
N(1)–Ru–N(6)	89.9(5)	N(2)–Ru–N(3)	90.5(5)
N(2)–Ru–N(4)	96.9(5)	N(2)–Ru–N(5)	173.3(5)
N(2)–Ru–N(6)	96.6(5)	N(3)–Ru–N(4)	80.2(5)
N(3)–Ru–N(5)	95.3(5)	N(3)–Ru–N(6)	172.6(5)
N(4)–Ru–N(5)	87.4(5)	N(4)–Ru–N(6)	96.5(5)
N(5)–Ru–N(6)	77.9(5)	O(1)–Ni–O(2)	82.8(5)
O(1)–Ni–N(7)	95.5(5)	O(1)–Ni–N(8)	171.3(5)
O(2)–Ni–N(7)	172.0(5)	O(2)–Ni–N(8)	96.3(5)
N(7)–Ni–N(8)	86.6(5)	N(7)–C(5)–C(6)	115.2(12)
N(8)–C(6)–C(5)	112.8(11)		

Table 3. Electrochemical Data ($E_{1/2}$/V vs Fc/Fc^+)[a)]

Compound	Oxidation 1	Oxidation 2	Reduction[b)]
1	+1.01		
2a	+0.87	+0.52	−1.38
2b	+0.94		−1.14
$[Ru(bpy)_3]Cl_2$	+0.88		
$[Ni^{II}(saloph)]$	+0.55		−1.82
$[Cu^{II}(saloph)]$			−1.57

a) The cyclic voltammetry was conducted with glassy C, Pt and Ag/Ag^+ as working, counter and reference electrodes, respectively, under a N_2 atmosphere. The concentration was kept at 1 mM in CH_3CN with 0.1 M TBAP. Scan rate = 100 mV/s. b) Peak potentials.

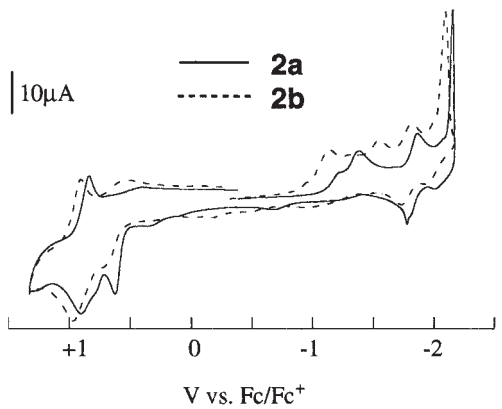

Fig. 2. Cyclic voltammograms of **2a**,**b** (1 mM) in CH_3CN (0.1 M TBAP) at a grassy carbon electrode vs Fc/Fc^+ internal reference. Scan rate = 100 mV s^{-1}.

bond length (2.06(1) Å) close to the normal range for $[Ru(bpy)_2(phen)]^{2+}$ (bpy = 2,2′-bipyridine, phen = 1,10-phenanthoroline).[18] The Ni(II) center has an approximately square-planar low-spin four-coordinate structure. The average Ni–N and Ni–O bond lengths are 1.86(1) Å and 1.84(1) Å, respectively, which are in agreement with those of $[Ni^{II}(saloph)$; saloph = *N*,*N*′-*o*-phenylenebis(salicylidenaminato)], respectively.[19] The spatial distance between Ru and Ni is 7.88(1) Å.

Electrochemical Studies. The electrochemical data for all of the complexes are summarized in Table 3. Cyclic voltammograms of **2a**,**b** are shown in Fig. 2. **2a** and **2b** show quasi-reversible redox waves at +0.87 and 0.94 V vs Fc/Fc^+ for the Ru(II)/Ru(III), respectively, which are almost equal to that of **1**. The reduction potentials, both of the Ni(I)/Ni(II) for **2a** (−1.38 V) and Cu(I)/Cu(II) for **2b** (−1.14 V), are observed more positively than those of $[Ni^{II}(saloph)]$ (−1.82 V) and $[Cu^{II}(saloph)]$ (−1.57 V), respectively. This may be due to the conventional substituent inductive effect upon the coordinated ruthenium(II) ion. Thus, the positively charged ruthenium(II) polypyridyl group should exert a substantial electron-withdrawing effect,[20] making the reductions of the Ni(II)/Ni(I) and Cu(II)/Cu(I) easier, and thereby shifting $E_{1/2}$ in the positive directions.

Absorption Spectra. The absorption spectra of **1**, **2a–c** and the reference compounds are shown in Fig. 3, and the data are summarized in Table 4. Assignments of the absorption

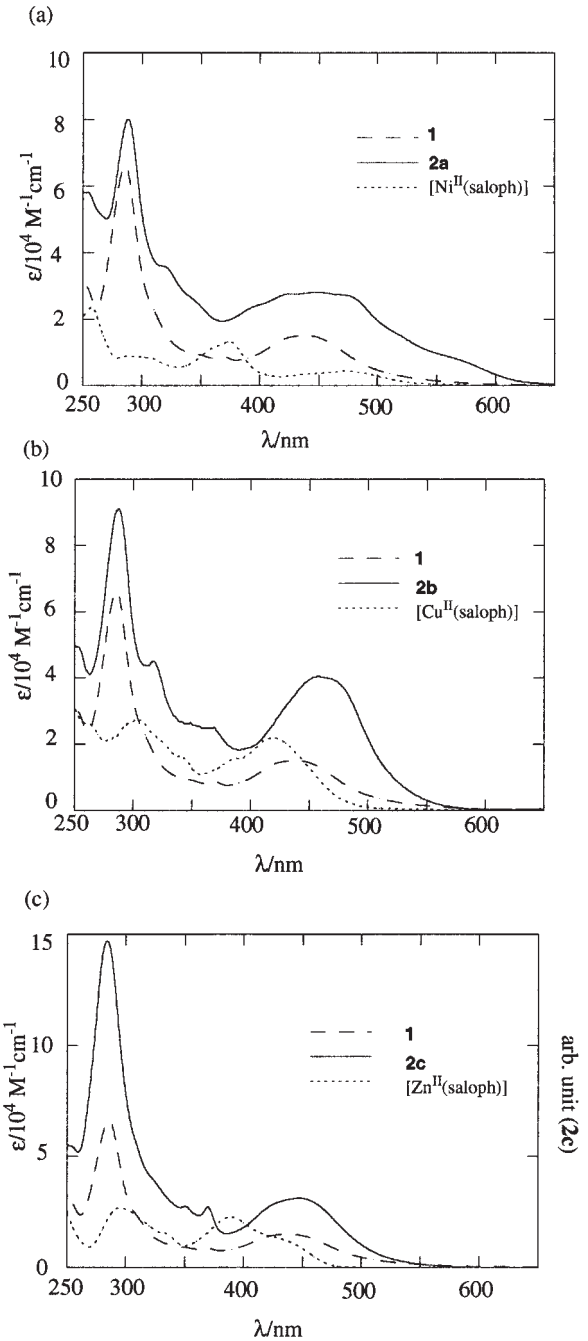

Fig. 3. (a) Absorption spectra of **1**, **2a** and $[Ni^{II}(saloph)]$, (b) **1**, **2b** and $[Cu^{II}(saloph)]$, (c) **1**, **2c** and $[Zn^{II}(saloph)]$ in CH_3CN except for $[Zn^{II}(saloph)]$ in CH_3CN. The ε of **2c** may be inaccurate due to impurity.

bands are made from the peak positions and intensities of MLCT (metal-to-ligand charge transfer) and LC (ligand-centered) transition bands observed for other ruthenium(II) polypyridyl complexes.[2] The absorption bands of **2a–c** in the 250–300 nm region are attributed to the LC transitions centered on the bipyridine ligand. The two broadened peaks observed in the region 300–400 nm for **2a** (λ_{max} 320, 340 nm), **2b** (λ_{max} 318, 349 nm) and **2c** (λ_{max} 351, 370 nm) can be assigned to the LC transitions centered on the bridging ligand, because such peaks are absent in the spectra of $[Ru(bpy)_3]Cl_2$

Table 4. Photochemical Data[a)]

Compound	Absorption λ_{max}/nm ($\varepsilon/10^4$ M^{-1} cm^{-1})	Emission[b)] λ_{max}/nm	τ/ns
1	243 (3.4), 286 (6.6), 350 (0.9sh), 367 (0.9sh), 438 (1.5)	620	980
2a	254 (5.8), 288 (8.0), 320 (3.6sh), 340 (2.7sh), 449 (2.8)	680	< 10
2b	254 (4.9), 287 (9.2), 318 (4.5), 349 (2.7sh), 458 (4.1)	660	80
2c	254, 284, 351, 370, 448	660	80
$[Ru(bpy)_3]Cl_2$	254 (2.2), 287 (8.5), 450 (1.5)	618	870
$[Ni^{II}(saloph)]$	258 (4.8), 289 (1.9), 374 (2.7), 474 (0.9)	—[c)]	
$[Cu^{II}(saloph)]$	261 (2.7), 306 (2.7), 419 (2.2)	—[c)]	
$[Zn^{II}(saloph)]$	242 (3.1), 295 (2.7), 389(2.3), 450 (1.4sh)	—[c)]	

a) Absorption and emission spectra were measured in CH_3CN except for [Zn(saloph)] in CH_3OH at room temperature. b) Emission spectra excited at 450 nm were corrected for spectral response by calibrating the fluorimeter with a standard lamp. The concentrations of all measured samples were 1.0×10^{-5} M. c) No emission.

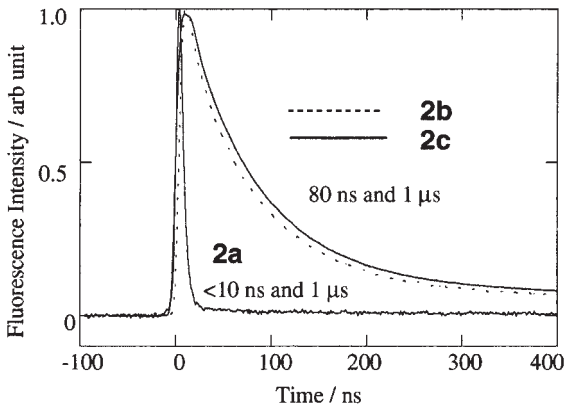

Fig. 4. Fluorescence decays of **2a–c** in CH_3CN excited at 532 nm and observed at 700 nm.

and the metal-Schiff base complexes, [M(saloph); M = Ni(II), Cu(II), Zn(II)]. Furthermore, the same absorptions are observed for the heteroleptic ruthenium(II) complexes having a bridging ligand, like tpphz (tetrapyrido[3,2-*a*:2′,3′-*c*:3″,2″-*h*:2″,3″-*j*]phenazine).[21] The absorption bands for **2a–c** in the 400–650 nm region include the MLCT transitions, and are more broadened compared to that of the mononuclear complex, **1**. This result suggests the presence of π-conjugation between the phenanthroline ring and the Schiff base unit. The extinction coefficients of the MLCT bands of **2a–c** are apparently larger than that of the mononuclear complex **1**. This may be due to the involvement of the absorption bands of the Ni(II)- (λ_{max} 474 nm), Cu(II)- (λ_{max} 419 nm) or Zn(II)-Schiff base unit (λ_{max} 389, 450 nm) into that of the ruthenium(II) component of **2a–c**.

Emission Spectra. As we have already reported, the emissions of **2a**,**b** are hardly detected with a steady-state luminescence spectrometer, since their intensities are considerably reduced to ca. 2% of that of $[Ru(bpy)_3]^{2+}$.[16] Two explanations might be possible for this result. One is the formation of a short-lived MLCT state which is different from that of $[Ru(bpy)_3]^{2+}$ (Ru(II)→bpy); the other is efficient quenching of the excited state by virtue of the intramolecularly attached the Ni(II)- or Cu(II)-Schiff base units.

In order to elucidate more precise photophysical behaviors, time-resolved measurements were carried out. The decay

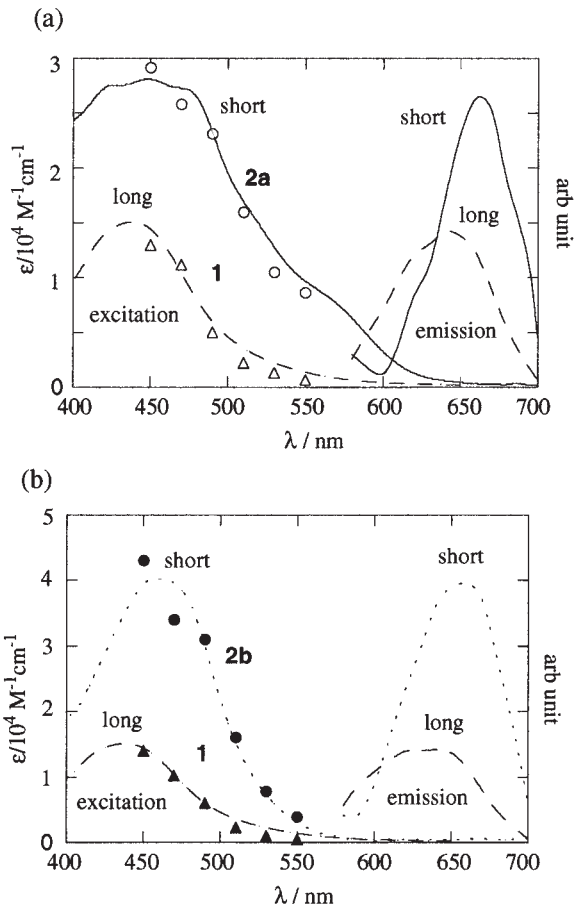

Fig. 5. Time-resolved excitation (λ_{obs} = 680 nm, ○ ● shorter-lived components, △ ▲ longer-lived component) and emission spectra (λ_{ex} = 500 nm, right side) in CH_3CN including absorption spectra (left side) of (a) **2a** (—), (b) **2b** (- - -), and **1** (— — —). Time-resolved excitation and emission spectra are arbitrary scale.

curves of the emission for **2a–c** observed in a CH_3CN solution at room temperature are shown in Fig. 4. The decay can be fitted by a double exponential function (**2a**; τ < 10 ns and 1 μs, **2b**,**c**; τ 80 ns and 1 μs). In order to distinguish two emission components, we plotted the amplitude of these components as a function of the wavelength (Fig. 5, emission).[22]

This result shows that the emission spectra of the short- and long-lived components are different from each other. The emission maxima of the short-lived species are observed at a longer wavelength (**2a**; λ_{max} 680 nm, **2b**; λ_{max} 660 nm) compared with those of the long-lived species (λ_{max} 620 nm). This indicates that the short- and long-lived species come from different emitted species.

In order to elucidate the origin of the emitted species, we analyzed the decay profiles (λ_{obs} 680 nm) recorded as a function of the excitation wavelength (Fig. 5, excitation).[23] Thus, the excitation spectra of the short- and long-lived species can be obtained, and these can be compared with the absorption spectra. The excitation spectra of the short-lived species are different from those of the long-lived species. Moreover, they are similar to the absorption spectra of **2a**,**b**, respectively, while the long-lived species are quite similar to the absorption spectrum of the mononuclear ruthenium(II) complex **1**, which is also shown in Fig. 5. Thus, it turns out that the short-lived species originated from the dinuclear complexes, **2a**,**b**. On the other hand, the luminescence of the long-lived species can be attributed to a small amount of the ruthenium(II) polypyridyl complexes carried through from the synthesis, since the emission lifetime of the longer one is almost equal to that of the mononuclear ruthenium(II) polypyridyl complexes,[2] and their emission intensity varied for each of the different samples of **2a**,**b**.[24]

In general, the Zn(II) analogues have an electrostatic effect similar to those of the Cu(II) and Ni(II) complexes, but cannot participate in either electron- or energy-transfer quenching, since the Zn(II) center lacks the d–d transition,[25] and therefore the lifetime of **2c** might indicate the intrinsic deactivation rate of the ruthenium(II) chromophore in these systems. The emission maximum of **2c** was shown at 660 nm, and the lifetime was found to be 80 ns. In the case of $[Ru(bpy)_3]^{2+}$, the emission (λ_{max} 620 nm) is already assigned to the Ru(II)→bpy MLCT state.[3] On the other hand, the emission peaks of **2a**–**c** are red-shifted from those of **1** and $[Ru(bpy)_3]^{2+}$. This clearly shows that the emissions of **2a**–**c** are supposed to come from the MLCT excited state due to the transition from Ru(II) to a ligand other than bpy, namely the transition of the Ru(II)→bridging ligand (herein after $MLCT_0$). The lifetime of **2b** (80 ns) is equal to that of the Ru(II)-Zn(II) analogue **2c**; namely, the 80 ns emission at 660 nm of **2b** can be considered to be residual emission from the $MLCT_0$ state. Furthermore, this suggests that no additional quenching process is likely to occur. On the other hand, in the case of **2a**, the lifetime (< 10 ns) is apparently shorter than that of **2c**, with indicates that some additional quenching process may proceed.

From a consideration of the redox potentials for **2a**,**b** described above, electron-transfer can be ruled out, since both of the Ni(I)/Ni(II) and Cu(I)/Cu(II) couples are very negative compared with $E_{1/2}$ for *Ru(II)/Ru(III).[26] Therefore, in the case of **2a**, energy-transfer, rather than electron-transfer, may take place as an additional quenching process.

The absorptions of **2a**,**b** at longer wavelength are supposed to contain the d–d transitions of the Ni(II)- or Cu(II)-Schiff base unit, since those of [Ni^{II}(saloph)] and [Cu^{II}(saloph)] are reported to appear at very low-energy regions.[11,27] Even though the extinction coefficients due to the d–d transitions for **2a**,**b** are very small, energy transfer could occur if the complexes have d–d transitions that match the excitation energy of the ruthenium(II) chromophore.[25] Therefore, the energy transfer from the $MLCT_0$ state to the d–d transitions of the metal-Schiff base unit could be expected to occur in both **2a**,**b**. However, this was not observed for **2b**; **2a** shows absorption at a longer wavelength (> 600 nm) than that of **2b** (Fig. 3). This implies that the energy level of the d–d transition state of **2a** is lower than that of **2b**. Although this difference is not always

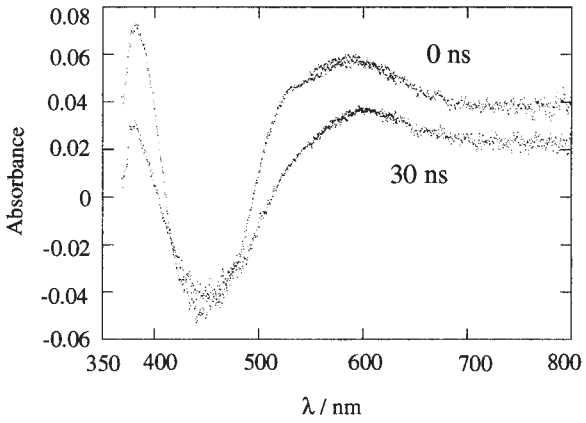

Fig. 6. Transient absorption spectra of **2b** at 0 and 30 ns after excitation at 355 nm in CH_3CN at room temperature.

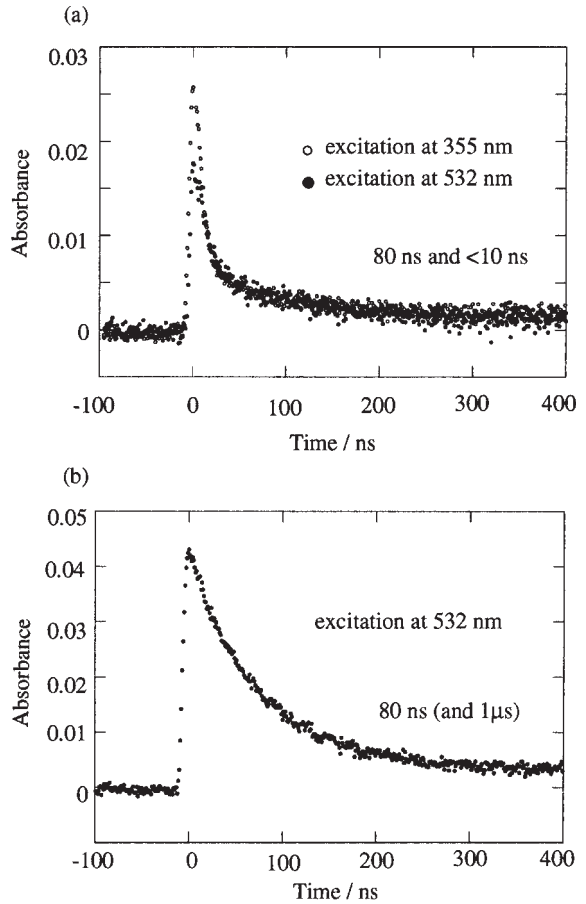

Fig. 7. Transient absorption signals of **2b** observed at (a) 525 nm and (b) 600 nm.

reflected for the energy level of the triplet state, energy-transfer from the $MLCT_0$ state may take place easily for **2a**, but not for **2b**.

Transient Absorption Spectra. The transient absorption spectra of **2b** at 0 and 30 ns after excitation are shown in Fig. 6. In these spectra, bleaching is observed in the 425–500 nm region, which reflects a decrease of the ground-state MLCT absorption. In addition, two weak absorption peaks at around 520 and 600 nm are observed at 0 ns, and the peak at 520 nm disappears after 30 ns. The time profiles of the transient absorption of **2b** observed at 525 and 600 nm are shown in Fig. 7. The decay rate of the absorption observed at 600 nm is 80 ns, which is the same as the luminescence lifetime of **2b**. The small component having a lifetime of 1 μs may come from the ruthenium(II) polypyridyl impurity, as already discussed. At 525 nm, the decay is composed of two lifetimes, < 10 ns and 80 ns. This indicates that another excited species having a short lifetime exist in addition to $MLCT_0$ (80 ns) and an impurity (~1 μs). As for the decay curve observed at 525 nm, the ratios of two components (80 ns and < 10 ns) are different from each other, depending on the excitation wavelengths, suggesting that these species are generated simultaneously under light irradiation. The decay of the transient absorption (Fig. 7a) shows that the shorter-component (< 10 ns) is predominant for excitation at 355 nm. This indicates that the different species of the excited states are generated depending on the excitation wavelength. As shown in Fig. 3b, the absorption by the Cu(II)-Schiff base unit is predominant at 355 nm, while the absorption by the ruthenium(II) polypyridyl group is predominant at 532 nm. Therefore, the shorter-lived component (< 10 ns) can be assigned to the absorption originating from the excited state of the Cu(II)-Schiff base unit, while the component having a lifetime of 80 ns can be assigned to the absorption originating from the $MLCT_0$ state (reaction 1 in Chart 1).

The transient absorption spectrum and the decay profile of **2a** are shown in Fig. 8 and Fig. 9, respectively. These spectra are different from those of **2b**. The transient absorption signal decays within the time resolution of our apparatus, indicating that the excited state decays with very short lifetime (< 10 ns). This may reflect fast energy-transfer from the $MLCT_0$ state to the Ni(II)-Schiff base unit. Consequently, the Ru(II)-Ni(II)* state, which is a product of the energy-transfer reaction, can be observed (reaction 2 in Chart 1). The bleaching at 550 nm corresponds to a loss of the ground state,[11] and the 500 nm transition can be assigned to short-lived absorption associated with the Ru(II)-Ni(II)* (Fig. 8). It could be analogous to the transition at 525 nm seen for the Ru(II)-Cu(II) dinuclear complex **2b**. These assignments are consistent with the fact that the d–d excited states do not live long.[25]

In general, energy transfer can be mediated either through a

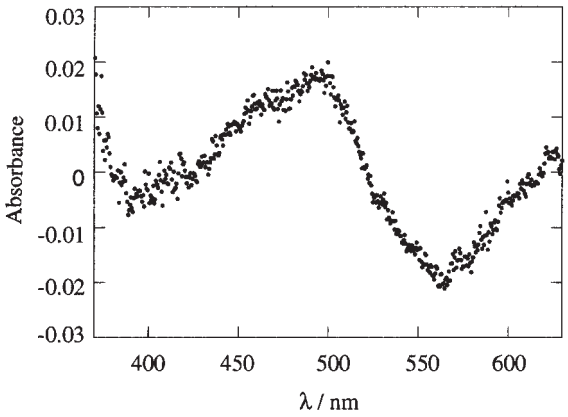

Fig. 8. Transient absorption spectrum of **2a** at 0 ns after excitation at 355 nm in CH_3CN at room temperature.

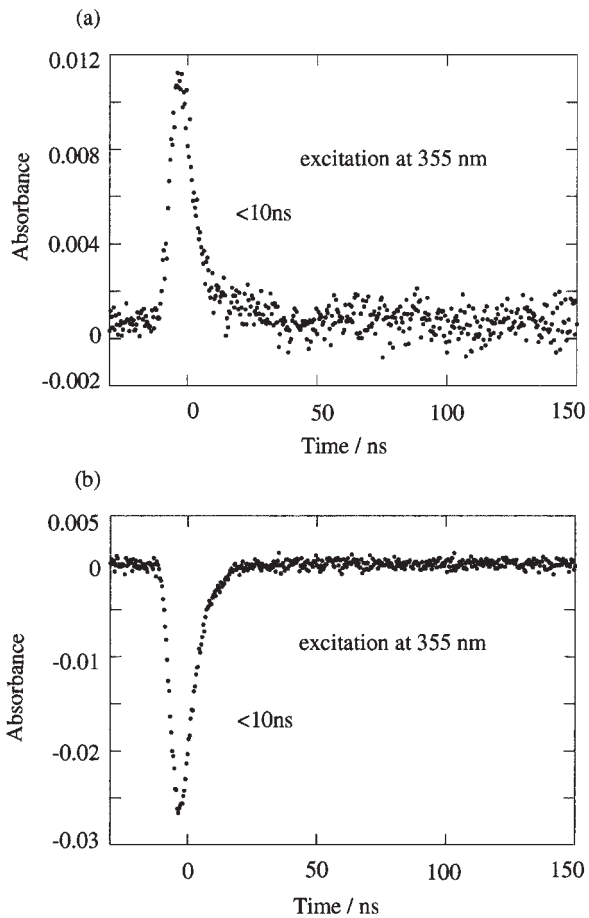

Fig. 9. Transient absorption signals of **2a** observed at (a) 450 nm and (b) 570 nm.

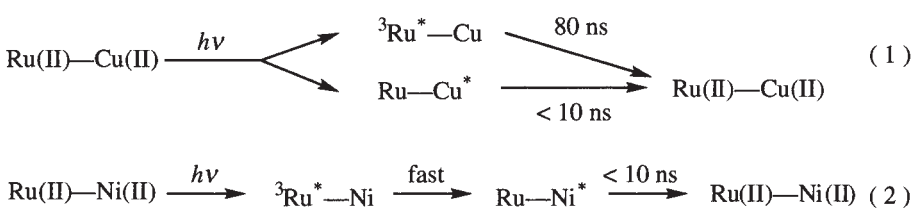

Chart 1.

dipole–dipole interaction (Forster's mechanism) or an exchange interaction (Dexter's mechanism). In view of the presence of a heavy atom in both the ruthenium(II) chromophore and the Ni(II)-Schiff base unit of **2a**, the latter seems to be the most likely. Dexter's mechanism can be viewed as a dual electron-transfer process, necessitating an orbital overlap between the excited state of the chromophore and the quencher.[25] Because of spatial distance between Ru and Ni is very close in the crystal structure of **2a**, the required orbital overlap will exist.

In both **2a**,**b**, no transient absorption could be observed after 100 ns. This indicates that long-lived charge-separated species are not generated in both systems. Therefore, the direct application of these dinuclear complexes to photochemical reactions seems to be rather difficult, although the experimental conditions for such reactions differ from those in the present work.

Conclusion

We have prepared novel Ru(II)-Ni(II) and Ru(II)-Cu(II) dinuclear complexes **2a**,**b**, in which the ruthenium(II) polypyridyl group and the Ni(II)- or Cu(II)-Schiff base units are fused together. Photochemical studies have revealed that the luminescence behaviors of the Ru(II)-Ni(II) and Ru(II)-Cu(II) dinuclear complexes are different from each other. Energy transfer from the excited state of the ruthenium(II) chromophore ($MLCT_0$) to the Ni(II)-Schiff base unit is likely to occur, though that from $MLCT_0$ to the Cu(II)-Schiff base unit may not. In both cases, the formation of a long-lived charge-separated intermediate was not observed. These facts imply that the dinuclear complexes **2a**,**b** may not be applicable to the photoreaction system directly. For realizing such systems, efforts to modify the structure of the complexes are now under way.

Experimental

All of the synthetic reactions were carried out under a nitrogen atmosphere. The melting points were measured on a Mettler FP62, and were uncorrected. ^{1}H NMR spectra were measured at 300 MHz in CD_3CN on a Varian Gemini 300 BB spectrometer, using tetramethylsilane (TMS) as an internal standard. The *J*-values are given in Hz. Electrospray ionization mass spectrometry was performed with a Micromass QUATTRO II spectrometer. An elemental analysis was carried out using an Eager 200 instrument. Unless stated, commercial-grade chemicals were used without further purification. A mononuclear Ru(II) complex **1** was prepared by the reported method.[17] [M(saloph)] (M = Ni(II), Cu(II), Zn(II)) was prepared according to a literature procedure.[28] (*Warning*: Because the perchlorate salts used in this study may be explosive and potentially hazardous, one should handle them with special care.)

Preparation of Ru(II)-Ni(II) Dinuclear Complex (2a). Mononuclear ruthenium(II) complex **1** (250 mg, 0.30 mmol) was reacted with nickel(II) acetate (75 mg, 0.30 mmol) and two equivalents of salicylaldehyde (74 mg, 0.60 mmol) in 20 mL of EtOH. After refluxing for about 8 h, the resulting mixture was evaporated to give a dark-red solid, which was dissolved in 10 mL of water. To this solution, a dropwise addition of lithium perchlorate (160 mg, 1.50 mmol) in water produced red precipitates, which were purified by column chromatography on alumina with a CH_3CN/H_2O/sat. KNO_3 aqueous solution (v/v/v = 100/10/1) as an eluate. A dark-red product was obtained in 47% yield (154 mg). mp > 250 °C (dec). Anal. Calcd for $C_{46}H_{32}N_8O_{10}Cl_2RuNi\cdot H_2O$: C, 49.98; H, 3.10; N, 10.14%. Found: C, 49.80; H, 3.22; N, 10.02%. ESIMS *m*/*z* 987 $[M - ClO_4]^+$. ^{1}H NMR (300 MHz, CD_3CN) δ 8.77 (d, $J = 8.5$ Hz, 2H), 8.57 (t, $J = 8.4$ Hz, 4H), 8.44 (s, 2H), 8.16–8.02 (m, 6H), 7.86 (d, $J = 4.9$ Hz, 2H), 7.74 (d, $J = 5.8$ Hz, 2H), 7.66 (d, $J = 8.5$ Hz, 1H), 7.64 (d, $J = 8.5$ Hz, 1H), 7.51–7.42 (m, 4H), 7.37–7.32 (m, 2H), 7.19–7.15 (m, 2H), 6.63 (t, $J = 7.0$ Hz, 2H), 6.39 (d, $J = 8.8$ Hz, 2H).

Preparation of Ru(II)-Cu(II) Dinuclear Complex (2b). This compound was synthesized following the same method as for **2a** using copper(II) acetate instead of nickel(II) acetate, and obtained as a dark-red powder. Yield 36%. mp > 250 °C (dec). Anal. Calcd for $C_{46}H_{32}N_8O_{10}Cl_2RuCu\cdot 2H_2O$: C, 48.97; H, 3.22; N, 9.93%. Found: C, 48.72; H, 3.14; N, 9.84%. ESIMS *m*/*z* 994 $[M - ClO_4]^+$.

Preparation of Ru(II)-Zn(II) Dinuclear Complex (2c). This compound was synthesized following the same method as for **2a** using zinc(II) acetate instead of nickel(II) acetate, though purification by column chromatography on alumina was incomplete because of instability. The product was recrystallized from CH_3OH, and obtained as an orange powder. Yield 21%. mp > 250 °C (dec). Anal. Calcd for $C_{46}H_{32}N_8O_{10}Cl_2RuZn\cdot 4H_2O$: C, 47.37; H, 3.46; N, 9.61%. Found: C, 47.86; H, 3.06; N, 9.19%. ESIMS *m*/*z* 995 $[M - ClO_4]^+$.

Electrochemical Measurements. Cyclic voltammetric measurements were performed with an ALS606 instrument in CH_3CN with 0.10 M tetrabutylammonium perchlorate (TBAP) as a supporting electrolyte, and the solution was bubbled with pure nitrogen gas saturated with CH_3CN. A three-electrode system was used: a glassy carbon electrode as the working electrode, a Pt wire as the counter electrode, and an Ag/Ag^+ electrode (BAS Co.) as the reference electrode. Ferrocene was used as an internal reference. Cyclic voltammograms, with a scan rate of 100 mV/s, were evaluated graphically. The concentrations of all sample solutions were kept at 1.0 mM.

X-ray Crystallography. The crystal data for **2a** was collected at room temperature in the $\theta/2\theta$ scan mode with a crystal of $0.45 \times 0.10 \times 0.20$ mm^3 dimensions on a Mac Science MXC18 diffractometer using graphite-monochromated Mo Kα ($\lambda = 0.71073$ Å). The experimental data are given in Table 1. A total of 8172 independent reflections were collected over the range $3° < \theta < 50°$; 3788 ($|F_o| \geq 3\sigma|F_o|$) reflections were used. The structure was solved by a direct method and refined by full-matrix least-square techniques. All of hydrogen atoms were included at calculated positions with fixed thermal parameters. All non-hydrogen atoms were refined anisotropically. Crystallographic data have been deposited at the CCDC, 12 Union Road, Cambridge CB2 1EZ, UK and copies can be obtained on request, free of charge, by quoting the publication citation and the deposition number 182808.

Photochemical Measurements. Absorption and luminescence spectra were measured with a Jasco V-550 spectrometer and a Hitachi F-4500 spectrofluorimeter, respectively. The time profiles of the fluorescence were measured with a nanosecond pulsed laser. Laser light pulses of various wavelengths were generated with an optical parametric oscillator (Continuum, Surelite OPO) pumped with a Nd^{3+}:YAG laser (Continuum, Surelite II). The pulse duration of the laser was 8 ns. The fluorescence from a sample in a 1 cm quartz cell was detected with a photomultiplier (Hamamatsu, R928) after being dispersed by a monochromator

(JASCO, CT-10). The signals were processed with a digital oscilloscope (Tektronix, TDS680C) and analyzed with a computer. For measurements of the transient absorption, a 3rd-harmonic pulse (355 nm) from a Nd^{3+}:YAG laser (Continuum, Surelite II) was used as the pumping light. The pulse duration of the laser was 8 ns. The sample solution was put into a 1 cm quartz cell. A Xe flash lamp (Hamamatsu, L4642, 2 ms pulse duration) was used as the probe light source. The spectrum of the probe light transmitted through the sample was measured simultaneously with a gated CCD camera (Roper Scientific, ICCD-MAX) after being dispersed by a monochromator (Roper Scientific, SP-308) controlled with a computer. For measurements of the decay profiles, the probe light was detected by a photodiode with a monochromator (JASCO, CT-10). A Si-photodiode (Hamamatsu, S-1722) was used for detection. Signals were processed with a digital oscilloscope (Tektronix, TDS680C) and analyzed by a computer.

References

1 F. Scandola, M. T. Indelli, C. Chiorboli, and C. A. Bignozzi, *Top. Curr. Chem.*, **158**, 73 (1990); M. D. Ward, *J. Chem. Educ.*, **78**, 321 (2001).

2 W. R. McWhinnie and J. D. Miller, *Adv. Inorg. Chem. Radiochem.*, **12**, 135 (1969); A. Juris, V. Balzani, F. Barigelletti, S. Campagna, P. Belser, and A. von Zelewsky, *Coord. Chem. Rev.*, **84**, 85 (1988).

3 D. M. Roundhill, ''Photochemistry and Photophysics of Metal Complexes,'' Plenum Press, New York (1994), pp. 165–210.

4 V. Balzani and F. Scandola, ''Supramolecular photochemistry,'' Horwood: Chichester, U. K. (1991), pp. 51–75; V. Balzani, A. Juris, M. Venturi, S. Campagna, and S. Serroni, *Chem. Rev.*, **96**, 759 (1996); F. Barigelletti and L. Flamigni, *Chem. Soc. Rev.*, **29**, 1 (2000).

5 M. Milkevitch, H. Storrie, E. Brauns, K. J. Brewer, and B. W. Shirley, *Inorg. Chem.*, **36**, 4534 (1997).

6 D. Gust, *Nature*, **372**, 133 (1994); J.-M. Lehn, ''Supramolecular Chemistry,'' VCH, Weinheim (1995), pp. 89–135; P. Belser, S. Bernhard, C. Blum, A. Beyeler, L. De Cola, and V. Balzani, *Coord. Chem. Rev.*, **190–192**, 155 (1999).

7 L. M. Dupray and T. J. Meyer, *Inorg. Chem.*, **35**, 6299 (1996); M. Suzuki, S. Kobayashi, M. Kimura, K. Hanabusa, and H. Shirai, *Chem. Commun.*, **1997**, 227; L. M. Dupray, M. Devenney, D. R. Striplin, and T. J. Meyer, *J. Am. Chem. Soc.*, **119**, 10243 (1997).

8 E. Kimura, X. Bu, M. Shionoya, S. Wada, and S. Maruyama, *Inorg. Chem.*, **31**, 4542 (1992).

9 N. Komatsuzaki, Y. Himeda, T. Hirose, H. Sugihara, and K. Kasuga, *Bull. Chem. Soc. Jpn.*, **72**, 725 (1999).

10 G. J. Kavarnos and N. J. Turro, *Chem. Rev.*, **86**, 401 (1986).

11 M. D. Hobday and T. D. Smith, *Coord. Chem. Rev.*, **9**, 311 (1972).

12 E. N. Jacobsen, I. Markó, W. S. Mungall, G. Schröder, and K. B. Sharpless, *J. Am. Chem. Soc.*, **110**, 1968 (1988).

13 M. Watkinson, A. Whiting, and C. A. McAuliffe, *J. Chem. Soc., Chem. Commun.*, **1994**, 2141.

14 S. Gambarotta, F. Arena, C. Floriani, and P. F. Zanazzi, *J. Am. Chem. Soc.*, **104**, 5082 (1982).

15 A. A. Isse, A. Gennaro, E. Vianello, and C. Floriani, *J. Mol. Cat.*, **70**, 197 (1991).

16 A part of the study has already appeared as a communication; N. Komatsuzaki, Y. Himeda, M. Goto, K. Kasuga, H. Sugihara, and H. Arakawa, *Chem. Lett.*, **1999**, 327.

17 E. Ishow, A. Gourdon, and J.-P. Launay, *Chem. Commun.*, **1998**, 1909.

18 B.-H. Ye, X.-M. Chen, T.-X. Zeng, and L.-N. Ji, *Inorg. Chim. Acta*, **240**, 5 (1995).

19 A. Radha, M. Seshasayee, K. Ramalingam, and G. Aravamudan, *Acta Crystallogr. Sect. C*, **41**, 1169 (1985).

20 C. B.-Brennan, P. Subramanian, M. Absi, C. Stern, and J. T. Hupp, *Inorg. Chem.*, **35**, 3719 (1996).

21 J. Bolger, A. Gourdon, E. Ishow, and J.-P. Launay, *Inorg. Chem.*, **35**, 2937 (1996); S. Kelch and M. Rehahn, *Macromolecules*, **30**, 6185 (1997); S. Campagna, S. Serroni, S. Bodige, and F. M. MacDonnell, *Inorg. Chem.*, **38**, 692 (1999).

22 The resolved amplitudes of a two-exponential fit were plotted as a function of the observed wavelength (λ_{ex} 500 nm). The spectra were reconstructed from fits to the decays collected at 13 wavelengths and corrected for the detector sensitivity.

23 The resolved amplitudes of the two-exponential fit were plotted as a function of the excitation wavelength (λ_{obs} 680 nm). The spectra were reconstructed from fits to the decays collected at 6 wavelengths and corrected for the detector sensitivity.

24 Though recrystallization was repeatedly done, a pure sample could not be obtained. A trace of ruthenium(II) polypyridyl impurity, which has been carried through the synthesis, is known to have almost no effect on the measurement result.[29] Therefore, we considered that this impurity could be safely ignored.

25 S. C. Rawle, P. Moore, and N. W. Alcock, *J. Chem. Soc., Chem. Commun.*, **1992**, 684.

26 The Ru(II)-Ni(II) dinuclear complex **2a** has 1.84 eV of the MLCT excited energy, calculated from the wavelength of the emission maxima (680 nm) in CH_3CN. As a result, $E_{1/2}$ for *Ru(II)/Ru(III) becomes $E_{1/2}$(*Ru(II)/Ru(III)) = $E_{1/2}$(Ru(II)/Ru(III)) $- E_{MLCT} = -0.97$ V vs Fc/Fc^+. The excited state, *Ru(II), the oxidation potential of which is -0.97 V, as estimated above, is unlikely to reduce the Ni(II)-Schiff base part ($E_{1/2}$(Ni(II)/Ni(I)) $= -1.38$ V vs Fc/Fc^+. In the case of **2b**, the excited ruthenium(II) chromophore could also not donate an electron to the attached Cu(II)-Schiff base unit for the same reason.

27 E. Suresh, M. M. Bhadbhade, and D. Srinivas, *Polyhedron*, **15**, 4133 (1996).

28 C. S. Marvel, S. A. Aspey, and E. A. Dudley, *J. Am. Chem. Soc.*, **78**, 4905 (1956).

29 X. Song, Y. Lei, S. Van Wallendal, M. W. Perkovic, D. C. Jackman, J. F. Endicott, and D. P. Rillema, *J. Phys. Chem.*, **97**, 3225 (1993).